ADVANCED FUNCTIONAL MATERIALS
www.afm-journal.de

A Facile Scalable Strategy for Constructing Novel Robust Self-Healing Glove Utilizing Nanoreinforced Thermoreversible Carboxylated Nitrile Butadiene Rubber

*Darren Yi Sern Low, Janarthanan Supramaniam, Bey Hing Goh, Sivakumar Manickam, and Siah Ying Tang**

Recent decades have seen an increase in using self-healing technology in fabricating multifunctional rubber materials, which incorporate intrinsic mechanisms. However, achieving commendable self-healing efficiency while maintaining strength in thin rubber films remains challenging. Herewith, the preparation of self-healing carboxylated nitrile butadiene rubber thin films is presented with 0.40 ± 0.05 mm thickness, reinforced with sustainable TEMPO-oxidized cellulose nanofibers. The thin films are fabricated using wet mixing and casting methods and translated to prototype fabrication via dipping. The study involves the effect of varying zinc stearate and filler concentrations on healing efficiency via ionic mechanisms alongside other characterization techniques, such as chemical composition, surface morphology, cross-link density, and thermal stability. The fabricated thin films exhibited a tensile strength of 5.38 MPa and an elongation-at-break of 518%. After undergoing a temperature-induced healing process at 100 °C for 1 h, the healing efficiency for both properties reached 72% and 90%, respectively. Moreover, these films demonstrates the ability to heal repeatedly at the same fracture site over multiple cycles, maintaining a healing efficiency of over 45% after the third cycle. A glove prototype is fabricated and tested using water and air leakage tests to prove the self-healing technology's successful transfer.

1. Introduction

Global urbanization, economic growth, and an increase in population are key contributors to waste generation. From the billions of tonnes of solid waste generated annually in the past decade, 9.2 million tonnes of rubber waste were accounted for, and only less than 20% of it was recycled.[1] With the continuous rise in global demand for rubber products, particularly single-use and disposable ones, exacerbated by the recent pandemic, there is a significant surge in waste accumulation in landfills. Moreover, as manufacturers worldwide shift toward synthetic rubbers like nitrile butadiene rubber (NBR) and its derivatives, the environmental impact of their waste becomes even more pronounced. To address this, various initiatives have been implemented to enhance the sustainability of rubber products. These include efforts to accelerate their biodegradation rates,[2,3] mitigate harmful emissions throughout the

D. Y. S. Low, S. Y. Tang
Department of Chemical Engineering
School of Engineering
Monash University Malaysia
Jalan Lagoon Selatan, Bandar Sunway, Selangor Darul Ehsan 47500, Malaysia
E-mail: patrick.tang@monash.edu

J. Supramaniam, B. H. Goh
Biofunctional Molecule Exploratory Research Group (BMEX)
School of Pharmacy
Monash University Malaysia
Bandar Sunway, Selangor Darul Ehsan 47500, Malaysia

B. H. Goh
Sunway Biofunctional Molecules Discovery Centre (SBMDC)
School of Medical and Life Sciences
Sunway University
Subang Jaya, Selangor Darul Ehsan 47500, Malaysia

B. H. Goh
Faculty of Health
Australian Research Centre in Complementary and Integrative Medicine
University of Technology Sydney
Ultimo, NSW 2007, Australia

S. Manickam
Petroleum and Chemical Engineering Department
Faculty of Engineering
Universiti Teknologi Brunei
Bandar Seri Begawan BE1410, Brunei Darussalam

The ORCID identification number(s) for the author(s) of this article can be found under https://doi.org/10.1002/adfm.202401345

DOI: 10.1002/adfm.202401345

production lifecycle,[4,5] optimize manufacturing processes for efficiency,[6,7] and enhance material recyclability.[8] However, the rate of use and disposal outweighs the success of these measures. Nevertheless, technological advancements in polymer chemistry and chemical engineering may also play a role in conserving the environment. Self-healing technology is one of several approaches that are being explored to reduce environmental waste by improving the service life and durability of materials. Additionally, it can be easily integrated into rubber matrices to produce self-healing rubbers.[9–11]

Drawing inspiration from biological systems, autonomous self-healing rubbers represent a class of specialty polymers capable of repairing themselves following damage. This remarkable property opens diverse applications across various sectors, including automobile tyres, soft robotics, wearable electronics, medical devices, and personal protective equipment.[10,12–14] Self-healing rubber must be able to combine desirable mechanical strength and robustness without affecting its healing ability. Rubber matrices may be endowed with the capabilities of self-repairing and reprocessing if dynamic linkages are constructed within them. There remains, however, a formidable challenge in designing reversible rubber networks with high self-healing capabilities and mechanical performance.[15–17] This could be viewed from several perspectives, including the chemistry and interactions between polymer chains of the base material, the reversible mechanism deployed to achieve self-healing, and other physical factors (such as stimulus dependence and application-specific properties). It is essential to highlight that the additional energy required to initiate self-healing in materials and products, along with its relation to healing cycles, plays a significant role in determining the functional unit for healing.[18] A new generation of self-healing polymers can be formed by integrating self-healing technology into rubber matrices by developing and deploying mobile, reversible cross-linked networks.[19–21] Numerous inherent self-healing technologies have been implemented across various rubber latex formulations.[9,11,22,23] However, the end goal for all studies must remain the same, that is, to achieve high self-healing efficiency with little or no reliance on external stimuli, repeatable healing cycles, rapid response times, and scalability.

Despite the general feasibility of integrating self-healing technology into natural and synthetic rubbers, studies on carboxylated nitrile butadiene rubber (XNBR) and its potential self-healing properties were found to be lacking. In general, XNBR is a derivative of nitrile NBR, but it contains additional carboxyl groups along its hydrocarbon chain. Compared to NBR, it has greater strength, excellent abrasion and tear resistance, and good resistance to oils and solvents.[24] XNBR with varying zinc thiolate concentrations was studied by Zainol et al.[25] for use in heavy engineering applications based on its self-healing properties and recycling capabilities. With a zinc thiolate concentration of 30 PHR and a sample thickness of 3 mm, 98% of the tensile strength (8 MPa) was recovered after thermal healing at 150 °C for 10 min. Several other studies have also examined the effect of stearic acid and stearic metal compounds, such as zinc stearate (ZnSt), as a compounding agent in synthetic rubber (i.e., styrene-butadiene rubber (SBR)), on mechanical, self-healing, and shape retainment properties in tyres, sensors, and smart textiles.[26,27] In these studies, samples of 2 mm thickness were fabricated, and successful retainment of shape properties was observed. A further advantage of zinc moieties is that they can form strong ionic interactions, which are capable of providing self-healing properties to rubbers.[28–30] In a recent study, Wajge and Das[31] investigated ferric-carboxylate interactions facilitated by dimethylaminopyridine to enhance reversible cross-linking with recyclability. Similarly, Huang et al.[32] explored the integration of copper (II) and trivalent dysprosium ions (Dy^{3+}) to form triethylamine coordination complexes, resulting in a soft, self-healing conductor. Notably, both studies utilized XNBR as the base material substrate.

Given XNBR's versatility, it finds application in various products, including hoses, rubber belts, vibration absorbers,[33] seals, gaskets, soft robotic components[14] and thin barrier products like gloves. Furthermore, there is potential to incorporate self-healing technology into these products. While some scientific breakthroughs have been achieved, it has not been easy to control or standardize the physical dimensions of prepared specimens (e.g., contact cross-sectional area or interface) to match the possible applications of functional materials with self-healing technologies. As healing efficiency is influenced by the relative values between the initial and recovered stresses, it is crucial to consider the actual magnitude of the strength recovered and not solely the healing efficiency achieved. Additionally, it is important to note that a majority of studies report low magnitudes of recovered tensile strength, of about 1–2 MPa, which impedes industrial applications.[34,35] Contextually, the process of preparing and testing self-healing XNBR thin films under 1 mm thickness with high strength recovery and fabrication of a functional self-healing glove prototype has yet to be reported.

To address this research gap, this study focuses on the fabrication of thermally accelerated ionic cross-linked XNBR thin films. It explores how these films interact with varying zinc concentrations of zinc stearate (ZnSt) and synergize with a functionalized nanocellulose filler called TEMPO-oxidized cellulose nanofibers (TOCN). By combining established ionic networks with different zinc-based compounding agents and H-bonds, the study aims to enhance the self-healing properties of XNBR. The optimized formulation would then be applied to fabricate a self-healing glove prototype. Assessments were first made of the effects of ZnSt and, subsequently, filler concentration in the XNBR formulation on mechanical strength and self-healing efficiency after repeated fractures. The ZnSt compound, which contains stearate ions, possesses the unique property of changing phase at elevated temperatures and could form strong ionic cross-links between rubber polymer chains. The presence of additional surface carboxyl groups on the TOCN filler also enabled its dual role in improving initial strength and promoting recovery of ionic bonds through reversible interactions. It was envisaged that discoveries made through this study have great potential to be applied to industrial-scale glove manufacturing lines. Future research in this area could lead to the development of commercial products with self-healing properties, which would have significant market value and reduce resource consumption for sustainable manufacturing.

Table 1. Mechanical properties of XNBR thin films, sample size: n = 3.

Sample[a)]	Tensile Strength [MP]	Elongation-at-Break [%]	M100 [MPa]	M300 [MPa]	M500 [MPa]
XNBR-0ZnSt	8.31 ± 0.41	798 ± 25	1.86 ± 0.10	3.02 ± 0.18	4.61 ± 0.30
XNBR-0.5ZnSt	7.52 ± 0.54	796 ± 31	2.38 ± 0.27	3.57 ± 0.34	5.06 ± 0.47
XNBR-1ZnSt	7.04 ± 0.13	804 ± 34	1.92 ± 0.23	2.98 ± 0.27	4.38 ± 0.29
XNBR-2ZnSt	7.16 ± 0.03	772 ± 13	1.76 ± 0.09	2.95 ± 0.29	4.49 ± 0.20
XNBR-3ZnSt	7.43 ± 0.27	748 ± 53	1.92 ± 0.11	2.96 ± 0.29	4.44 ± 0.22
XNBR-4ZnSt	8.08 ± 0.20	780 ± 23	2.14 ± 0.20	3.42 ± 0.20	5.02 ± 0.31
XNBR-5ZnSt	8.58 ± 0.32	800 ± 39	2.41 ± 0.21	3.74 ± 0.17	5.41 ± 0.19

[a)] XNBR-*m*ZnSt, where *m* represents the amount of ZnSt added in PHR.

2. Results and Discussion

2.1. Fabricated Self-Healing XNBR Thin Films

The process of fabricating thin films through casting requires several observations. A thin film should be smooth without forming bubbles or foamy structures, fully gelated, and capable of being stripped off the Petri dishes in one piece with minimal to no residue. The formation of bubbles or porous textures causes inconsistencies in tensile strength measurements. Poor contact at the interface of fractured sites would also result in extremely low self-healing efficiencies.[36] The presence of voids also reduces the surface area of contact for self-healing, which represents a significant deterrent factor that should be eliminated. Due to this, a two-stage curing process of XNBR latex is necessary to prevent the water content from boiling and prevent the formation of voids during the gelation process.[37] In a slow cure process, the water content of the latex is removed, and the latex is gelated before it is cured at high temperatures to increase its strength and robustness. This strategy was successfully employed to cure all fabricated samples within the scope of the study to form smooth, thin films with controlled thickness. The experimental section provides detailed steps for preparing the self-healing XNBR thin films.

2.2. Effects of ZnSt Concentrations on XNBR Thin Films

2.2.1. Tensile Strength

Testing was conducted on all fabricated samples to quantify tensile strength (stress), elongation-at-break (strain), and modulus values. Representative stress–strain curves for each set of samples are presented in Figure S1 (Supporting Information), while **Table 1** presents the quantified mechanical properties of samples with varying ZnSt concentrations in the XNBR formulation. The study noted minimal impacts on the breaking point properties of XNBR, namely tensile strength and elongation-at-break values, across various formulations. The tensile strength of the XNBR composites remained consistently above 7 MPa, while elongation-at-break values ranged from 750% to 800%. Higher concentrations of ZnSt led to increased initial moduli, including modulus at 100% elongation (M100) and modulus at 300% elongation (M300). However, excessive ZnSt concentration (e.g., 15 PHR) exhibited adverse effects on the mechanical properties of rubber, such as reduced strengths and strains, likely attributed to its role as an anti-tacking agent and lubricant.[26] Nevertheless, a suggested threshold value of 5 PHR could still provide positive reinforcing effects without significantly impacting material elongation.[27,38,39] It might also be explained by ZnSt's phase-changeable or mechano-adaptive behavior, which switches at around 100–120 °C, functioning as an active reinforcement filler that provides strength at localized regions within the rubber matrix.[26,39]

2.2.2. Self-Healing Efficiency

In order to assess the self-healing efficiency of the thin films, the samples were cut in the middle with scissors. After separating the pieces, the exposed surfaces were brought back together and allowed to heal under elevated temperature of 100 °C for 1 h, benchmarked by studies conducted over a wide range of self-healing elastomers.[40,41] A further benefit of ZnSt's phase-changeability is that it occurs at high temperatures, which could yield higher self-healing efficiencies and magnitudes of recovered strengths.

In this study, XNBR-1ZnSt-SH1 exhibited the highest strength recovery value of 4.53 ± 0.37 MPa, resulting in a self-healing efficiency of approximately 64%, as shown in **Figure 1**a,b, respectively. Following closely were XNBR-2ZnSt-SH1, XNBR-3ZnSt-SH1, and XNBR-0.5ZnSt-SH1, with respective healing efficiencies of 52%, 46%, and 41%. Figure 1c depicts the stress–strain curve of the healed sample compared to that of the virgin XNBR-1ZnSt sample. The generic stress–strain curve shape was retained with higher modulus values until fracture. As a result of re-exposure to high temperatures, the samples would likely become brittle, increasing their strength and decreasing their elongation. The control sample (XNBR-0ZnSt) exhibited an approximate 35% self-healing efficiency. This observation could be attributed to the involvement of zinc oxide in facilitating dynamic reversible ionic interactions.[30] Furthermore, the presence of zinc diethyldithiocarbamate (ZDEC), in conjunction with ZnO, generates Zn^{2+} ions that react with the carboxylate groups of the XNBR, thereby forming ionic crosslinks between separate rubber chains. However, it is worth noting that the C—C and C—S bonds within the XNBR chains, as well as those with ZDEC, lack dipole moments, rendering them non-polar irreversible covalent bonds.[25] However, there is the possibility of enhancing the effectiveness of the healing process through the synergistic effects of ZnSt, which also contains zinc moieties. While the initial tensile strength determines self-healing efficiency, it is also important to consider the magnitude of recovered tensile strength and the

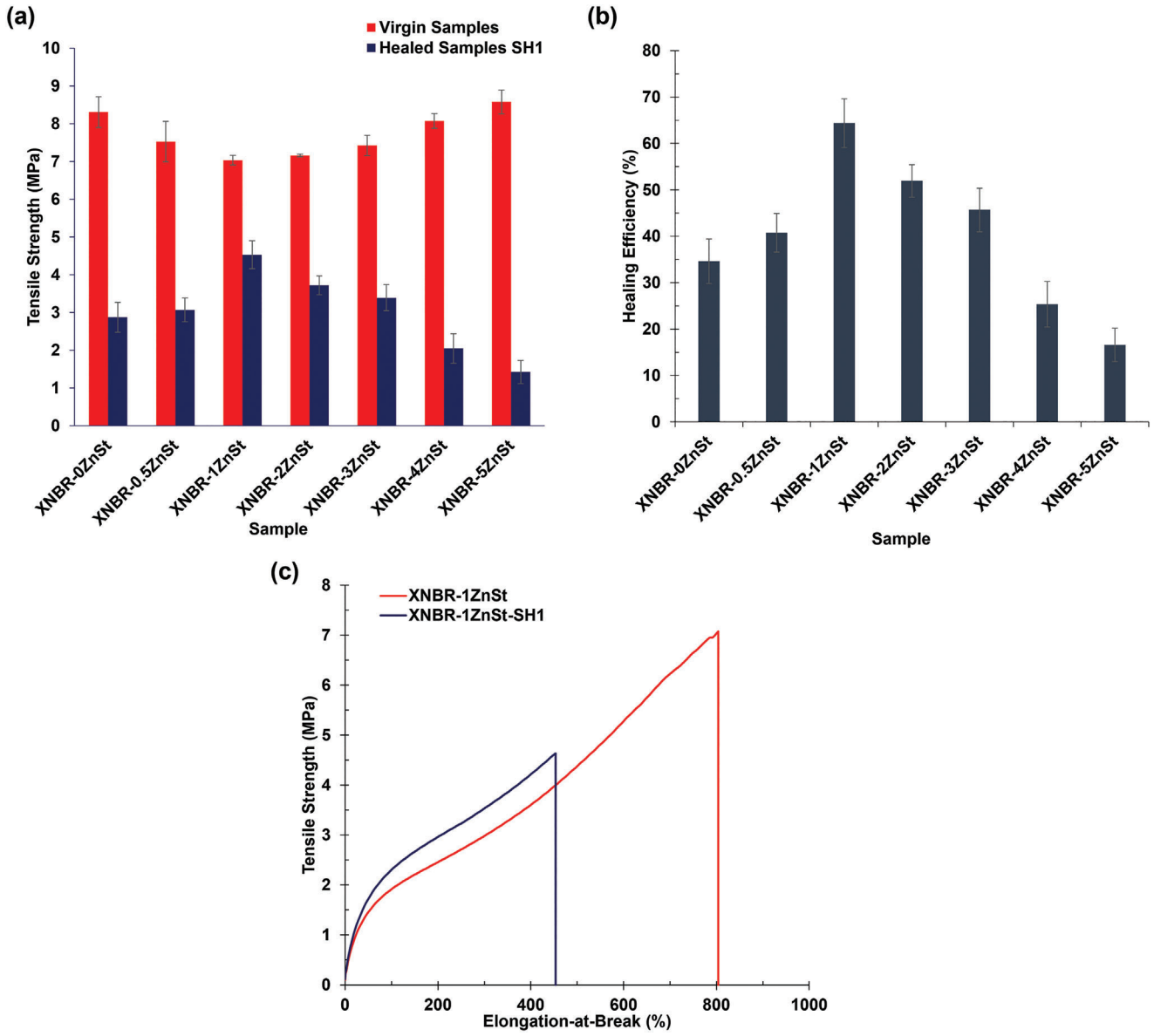

Figure 1. a) Recovered strength and b) Self-healing performance of samples after 100 °C for 1 h in the first cycle (-SH1), sample size: n = 3; c) Representative stress–strain curve of XNBR-1ZnSt and XNBR-1ZnSt-SH1.

thickness of the samples. It is theoretically feasible that a greater surface area exposed upon cut, damage, or fracture would allow for more bonds to recombine, resulting in a higher recovered strength value and a more efficient healing process.[20] However, in light of the intended application of gloves, the samples were set to have a thickness of approximately 0.40 mm, referenced against commercialized products in the market.

When exposed to elevated temperatures, an optimal concentration of ZnSt facilitates the mobility of rubber polymer chains. As a result, the rubber chains exposed at the cut's interface can move and re-join with other rubber chains due to intrinsic self-healing mechanisms, such as the formation of ionic bonds. With a ZnSt concentration of 1 PHR, the fabricated samples were elastic, not brittle, and demonstrated good self-healing properties. In addition, the healed samples could be flexed, twisted, and stretched, as illustrated in Figure S2 (Supporting Information). Moving forward, a concentration of 1 PHR ZnSt would be used to investigate the impacts of nanocellulosic filler loading on the strengths and healing efficiencies of the XNBR composite.

2.3. Effects of Nanocellulosic Filler Concentrations on XNBR Thin Films

2.3.1. Tensile Strength

As observed distinctively in Figure 1a, there is a slight decrease in initial tensile strength at 1 PHR of ZnSt loading. However, this increase in recovered strength was greater than the decrease in initial strength, hence resulting in a higher self-healing

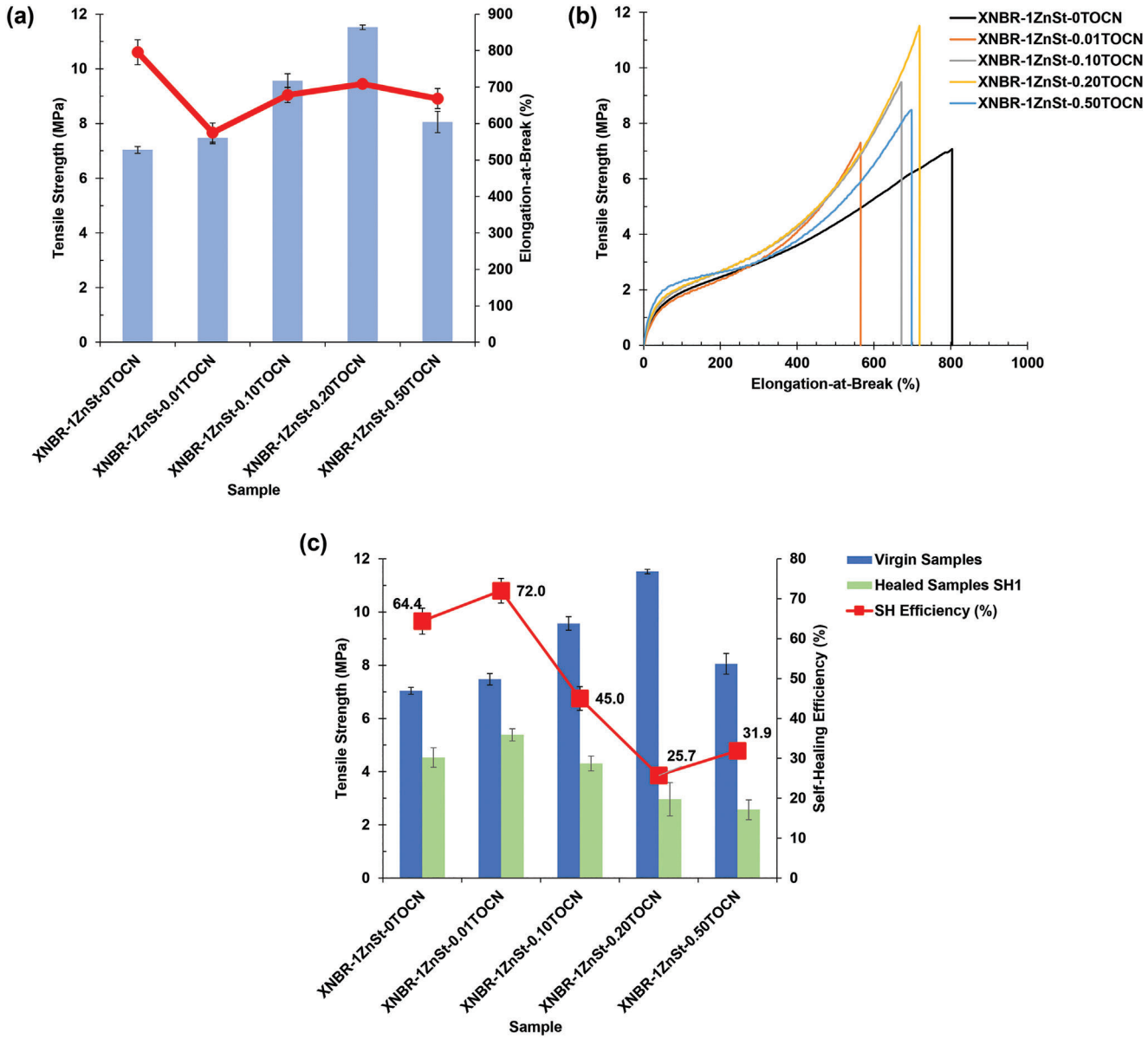

Figure 2. a) Tensile strength and elongation at break values and b) stress–strain curves of TOCN-filled XNBR composites; c) Magnitudes of initial tensile strength, recovered tensile strength, and self-healing efficiencies of TOCN-filled XNBR composites, sample size: n = 3.

efficiency. Ideally, a robust and durable rubber material bearing self-healing properties should possess high strengths before and after recovery, which remains challenging. To overcome this shortcoming, fillers such as nanocellulose represent an excellent candidate for rubber reinforcement as they possess high strengths and are renewable, sustainable and economical.[5,42,43] Therefore, with the as-determined latex formulation, the concentrations of TOCN filler were studied.

Figure 2a,b shows the stress values and stress–strain curves of the XNBR composites filled with varying concentrations of TOCN. Herewith, a general trend was observed, whereby the incorporation of nanocellulosic fillers improved the tensile strengths of samples at the expense of elongation.[5] This was attributed to the high strength of the filler itself, which was capable of withstanding and distributing loads more uniformly throughout the material till fracture. However, at higher filler loadings (i.e., 0.50 PHR), it was observed that there was a drop in tensile strength in the composite. When there is an overload of solid filler particles within rubber matrices, agglomeration occurs due to the hydrophobic nature of rubber matrices and the hydrophilic nature of nanocellulose, resulting in different polarities.[5] Consequently, stress points would form, causing uneven distribution of loads and leading to premature fracture.[44] Based on the findings, the addition of TOCN provided the best reinforcement at 0.20 PHR concentration, yielding tensile strengths of 11.52 ± 0.08 MPa and elongation values of ≈700%, suggesting that the composite is still flexible and remains suitable for glove applications.[43,45]

2.3.2. Self-Healing Efficiency

Self-healing efficiencies of the TOCN-filled XNBR composites were analyzed using the methodology mentioned above, with results shown in Figure 2c. When determining, comparing and analysing self-healing efficiencies, especially with filler reinforcements, several points should be noted. As shown in Equation (1), self-healing efficiency is a function that is inversely proportional to its initial tensile strength. This means that if the initial tensile strength were increased due to filler interactions, although with the same magnitude of strength recovered, the self-healing efficiency would suffer a decrease. Hence, it is important to compare the magnitude of recovered strengths, which is another crucial parameter to benchmark the value of rubber strength recovery. Therefore, it is of interest to explore fillers that could play dual roles, both in reinforcing and in providing more avenues to form reversible bonds, which dominate self-healing.

As observed, the addition of TOCN was advantageous to the composite's initial tensile strength due to reinforcement effects. However, it negatively affected the recovered tensile strength, resulting in an overall net decrease in self-healing efficiency. At a filler loading of 0.01 PHR, it was observed that both the initial and recovered tensile strength increased, with the latter showing higher magnitudes. This managed to increase the overall healing efficiency to 72.0%. This suggests that at low loadings of TOCN, the availability of carboxyl functional groups was effective in establishing more reversible ionic bonds. Upon further increasing filler loading, there was a decrease in recovered tensile strength attributed to the saturation of carboxyl groups and poor interactions at the fractured surfaces. At the upper limits of filler concentration, the initial tensile strength was negatively affected, caused by agglomeration and the formation of voids. However, the reduction magnitude outweighed that of the recovered tensile strength, resulting in a net increase in healing efficiency of 31.9%. This explains the importance of considering the magnitude of strength recovery in addition to healing efficiency to enable better judgement of feasibility in real-world applications.

When benchmarked with other literature studies in the field of self-healing XNBR composites, parameters such as sample thickness (interfacial contact dimensions), compounding formulation, healing conditions, and magnitudes of recovered strength were considered. **Table 2** lists a comparison of the results from this study with those of other recent reports. In this study, samples of significantly lower thickness (≈0.40 ± 0.05 mm) were prepared, resulting in a reduced cross-sectional contact area when the fractured specimens are reconnected, which would be beneficial for thin barrier or film applications, such as gloves. Additionally, while this study indicated a relatively lower self-healing efficiency, it is important to note that the magnitude of the initial and recovered tensile strength was higher than that of those with similar healing conditions. Optimizing these conditions (such as temperature and time) is a key consideration when comparing healing systems and their overall efficiency.

2.4. Cyclic Healing

A significant benefit of employing intrinsic mechanisms to achieve self-healing in materials is that repeated fractures could be treated at the same site.[52,53] Therefore, the rubber samples were tested to determine their cyclic healing potential and to quantify their healing efficiency. After tensile testing, the separated pieces were brought into contact again and subjected to the same thermal healing conditions before being tested. By repeating this cycle twice, each sample will have a total of three healing cycles, denoted with —SH1, —SH2, or —SH3. Measurements were triplicated in all cases. In **Figure 3**a,b, the self-healing efficiencies on varying ZnSt concentration and TOCN are shown over three healing cycles, calculated based on average initial tensile strength over average recovered strength. Additionally, Figure 3c,d shows the particular stress–strain curve that corresponds to XNBR-1ZnSt and XNBR filled with 0.01 PHR TOCN.

In all cases, findings indicate that healing efficiency gradually decreases after each cycle. The same trend has also been reported by Araujo-Morera et al.[27] Zhang et al.,[53] and Yan et al.[54] This is possibly due to the formation of microcracks and microtears during mechanical testing and environmental contamination by dust particles, which may prevent good contact between samples upon re-joining and negatively impact strength recovery.[20] XNBR-1ZnSt exhibited the highest self-healing efficiency after each fracture cycle, as shown in Figure 3a,c. Despite being exposed to elevated temperatures, the XNBR-1ZnSt sample continued to exhibit more than 50% healing efficiency after the second cycle and greater than 40% after the third cycle.

When TOCN fillers were added to the formulation, as shown in Figure 3b,d, a similar trend was observed, where healing efficiencies decreased over each cycle. At concentrations of TOCN beyond 0.01 PHR, the fillers possibly act as a hindrance for rubber polymer chains to re-join the supramolecular matrix, with more obvious deteriorating effects after each healing cycle. It was apparent that the addition of functionalized filler at low concentrations enabled improved self-healing efficiency by enhancing magnitudes of both initial and recovered tensile strengths. It was also clear that at this concentration, self-healing efficiencies were the highest between sets of the same cycle. Poorer healing efficiencies were observed onward, attributed to more significantly enhanced initial strengths over recovered strengths and saturation of carboxyl functional groups.

2.5. Microscopy

Figure 4a exhibits the stepwise microscopic images of XNBR-1ZnSt filled with 0.01 PHR of TOCN. It was observed that the gap created when the samples were cut and brought into contact had significantly reduced and was virtually indiscernible, as indicated by the arrows, demonstrating the occurrence of successful self-healing.[25,55] It has been possible to re-establish the cross-links between the zinc ions through thermal stimulus, which has allowed the material to regain its strength. In addition to allowing effective interdiffusion of rubber chains, heat has enabled the recovery of material properties.

The surface morphology of unfilled and filled XNBR-1ZnSt composite with TOCN are presented in Figure 4b,d. It can be observed that a relatively smooth morphology was obtained when the XNBR composite was compounded without fillers, indicating the absence of agglomeration and void formation during curing (Figure 4b). Figure 4c shows the compact fibrous structure of

Table 2. Review of recent studies on self-healing XNBR composites.

Rubber formulation/modification	Reference Sample	Thickness [mm]	Self-healing mechanism	Recovered strength [MPa][a)]	Healing Efficiency [%][a)]	Healing Duration	Healing Temperature [°C]	Refs.
Varying ZnSt	1 PHR ZnSt	0.40 ± 0.05	Ionic cluster interactions	*4.53 ± 0.40*	*64.4*	*1 h*	*100*	This study
Varying TOCN	*0.01 PHR TOCN*			5.38 ± 0.23	72.0			
Varying magnesium oxide (MgO)	1.25 MgO, Conventional	2	Ionic cluster interactions	≈26	>140	7 h	110	[14]
Varying triethylamine (T) and ferric chloride ($FeCl_3$)	20 mmol T, 6 mmol $FeCl_3$	Not stated	Metal-ligand coordination	3.9	≈90	24 h	70	[22]
Varying metal-cysteine complexes	1 PHR zinc-cysteine complex	Not stated	Metal-ligand coordination, disulfide interactions	3.4 ± 0.7	89.5	24 h	Room temperature	[23]
Varying zinc thiolate	30 PHR zinc thiolate	3	Covalent and ionic network	≈8	97.9	10 min	150	[25]
2,6-diaminopyridine ligand and divalent metal salts	4 PHR Co^{2+}	Not stated	Metal-ligand coordination	9.1 ± 1.3	88	24 h	80	[30]
	4 PHR Ni^{2+}			4.8 ± 1.1	56			
	4 PHR Zn^{2+}			4.4 ± 1.2	100			
Triethylamine-assisted ligand coordination complex with copper (Cu) and dysprosium (Dy) ions	[Cu:Dy] = 1:1 mol ratio	0.80	Metal-ligand coordination	≈5	93.6	1 h	80	[32]
Compounded with Fe_3O_4, $FeCl_3$ and 3,4-dihydroxybenzoic acid (DHBA)	10 PHR Fe_3O_4, 5 PHR $FeCl_3$, 5 PHR DHBA	0.50	Metal coordination bonds	≈6	66 ± 2	1 h	120	[46]
2,6-diaminopyridine, multi-walled carbon nanotubes (MWCNT) and zinc oxide (ZnO)	0 PHR MWCNT	1	Metal-ligand coordination	3.22 ± 0.30	72.5	24 h	80	[47]
Fe^{3+} addition	0.75 PHR Fe^{3+}	2	Metal-ligand coordination	≈3.5	≈87	10 min	100	[48]
ZnO, sulphur and ZDEC	1 PHR ZnO, 0.8 PHR sulphur, 0.7 PHR ZDEC	≈1	Ionic cross-linking	2.3	43	30 min	180	[49]
Ionic liquid functionalized with graphene oxide (IL-GO) and ZnO	3 PHR IL-GO, 1 PHR ZnO	Not stated	Ionic cluster interactions	5.2 ± 0.5	85.2	24 h	40	[50]
ZnO with acrylic acid-grafted ground tyre rubber (gGTR)	6 PHR ZnO, 6 PHR gGTR	Not stated	Ionic cluster interactions	≈7.5	≈70	10 min	100	[51]

[a)] Significant figures of recovered strength and healing efficiency are reported as is. Figures and illustrations were used to approximate these values if they were not explicitly reported in the article's original version.

TOCN, which had a ribbon-like shape, with surfaces intact and smooth, similar to that observed by Lin et al.[56] The length of these fibres was also found to be several hundred micrometres. Meanwhile, Figure 4d shows the successful embedment of these fillers within the rubber composite with homogenous dispersion; however, some agglomerated TOCN particles were observed, as indicated by the arrows.

2.6. Thermal Stability Behavior

As the manufacturing of gloves involves high temperatures during processing, it would therefore be essential to ensure that the addition of fillers does not affect the degradation temperatures of XNBR. The thermal stability of the samples, mainly XNBR-1ZnSt alongside those filled with 0.01 PHR TOCN, was analyzed to determine whether the addition of nanocellulosic fillers would impact the thermal stability of the composite. Adding nanocellulosic fillers to the composite reduced the degradation temperature from 437 °C to approximately 425 °C, as shown in **Figure 5**a,b and **Table 3**. A shift of the DTG peak toward a lower temperature and a higher derivative weight indicates that the XNBR composite has poorer thermal stability and lower resistance to aging due to a smaller percentage change in sample weight per unit of time.[57] It is common that the addition of nanocellulosic fillers slightly reduces the degradation temperature of composites, possibly attributed to percolation thresholds, critical volume fractions and agglomeration.[58] This was evident in Figure 5b (inset), where composites filled with TOCN had the highest rate of weight loss occurring at 425 °C. Although there is a decrease in degradation temperature upon TOCN addition, the nature of XNBR being stable up to 400 °C is sufficiently high to withstand general glove manufacturing processes.[59] Furthermore, the incorporation of a sustainable filler also resulted in a lower carbon residue percentage after the composite was incinerated at 900 °C.

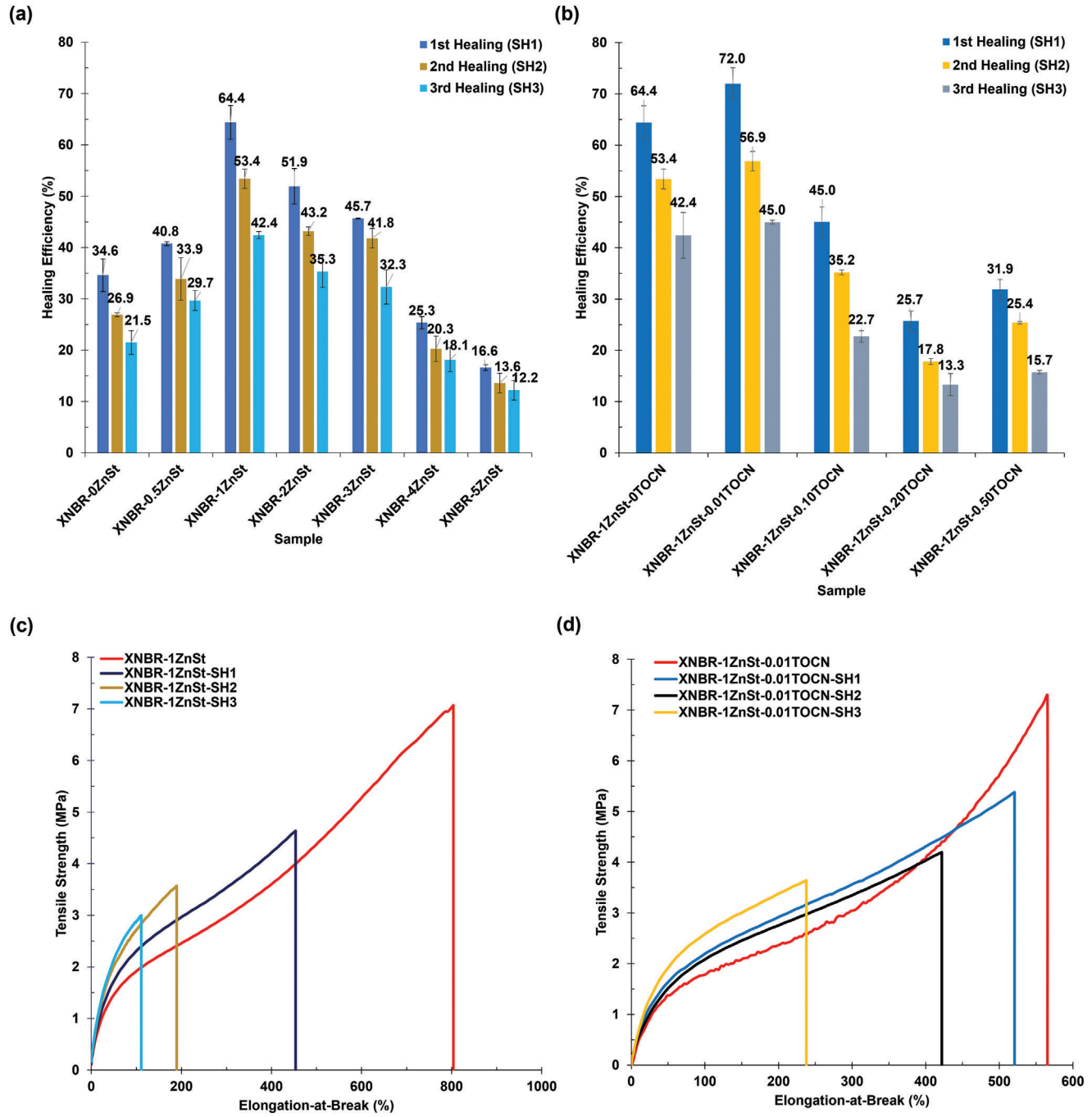

Figure 3. Healing efficiencies of up to three healing cycles of XNBR composites with varying a) ZnSt concentration; b) TOCN loading, sample size: n = 3; and representative stress-strain curves over three cycles for c) XNBR-1ZnSt; d) XNBR-1ZnSt filled with 0.01 PHR TOCN.

2.7. Chemical Interactions and Cross-Link Density

To investigate the possible chemical interactions between the ZnSt and fillers added to the compounding formulation with the XNBR matrix, Fourier-Transform infrared spectroscopy (FTIR) analysis was performed, as shown in **Figure 6a**. Broad peaks between wavenumbers 3200 and 3600 cm^{-1} are associated with the stretching vibrations of the OH— group. The TOCN filler has a peak at 2899 cm^{-1} from —CH stretching peaks and 1030 cm^{-1}, which corresponds to the C—O bonds of cellulose.[60,61] For XNBR composites, the peaks at 2924 cm^{-1} and 2849 cm^{-1} were attributed to asymmetric and symmetric stretching of CH— groups, respectively.[62] The composites also exhibited a common peak at 2236 cm^{-1}, resulting from a stretching vibration of its nitrile triple bond.[63] A slightly broader peak could be observed at 1598 cm^{-1} in the composite filled with TOCN, which suggested that there was more carbonyl stretching vibrations of zinc carboxylate salts, hence more ionic interactions, which promotes

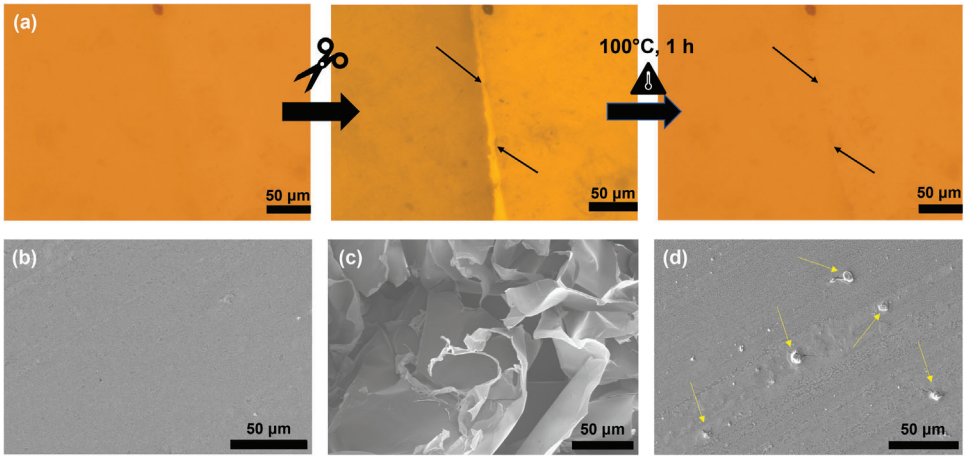

Figure 4. a) Stepwise optical microscopic images of XNBR-1ZnSt-0.01TOCN at pristine state, cut, and after self-healing; FE-SEM images of b) XNBR-1ZnSt; c) freeze-dried TOCN; d) XNBR-1ZnSt-0.01TOCN.

self-healing behavior.[64] A common peak at 1439 cm^{-1} is likely a result of the CH_2-bending vibrations of the scissoring bands of methylene, while 967 cm^{-1} represents a characteristic peak of CH-bending of the butadiene group.[65]

Using equilibrium swelling experiments, the cross-link density of the samples was quantified, with findings as shown in Figure 6b. In the first stage of equilibrium swelling, samples are immersed in toluene. This allows the determination of the total cross-links (sum of ionic and covalent) within the rubber network. The second stage of the swelling test involves the determination of ionic cross-link density by disrupting the covalent cross-links. In order to accomplish this, samples were re-immersed in a mixture of toluene and chloroacetic acid.[25] Once the solvent has been removed, the rubber chains will form a gel-like structure.[66] All samples were observed to maintain their opacity and shape during the first and second stages of swelling. This may be attributed to the dominance of covalent bonds in the overall cross-linking network.[37,67] Results obtained from the study indicate that ZnSt increased the overall cross-link density within the rubber matrix. In particular, ionic cross-link density increased significantly more than covalent cross-links, accounting for approximately 45% of the total cross-link density. This could further demonstrate the improvement in self-healing efficiency, as ionic bonds are responsible for bond reformation, which may lead to higher order aggregates following the Eisenberg model.[29,51,68] Furthermore, the high cross-link density of the samples could explain their high initial tensile strength between 7 and 8 MPa during mechanical testing. The incorporation of TOCN did not significantly affect the total cross-link density of the composites. However, it could be observed that the proportions between covalent and ionic cross-links were closer to being equalized. This would be beneficial for self-healing properties, as ionic cross-links are mainly responsible for recovery, while covalent cross-links dominate the strength and structure of the material.[37]

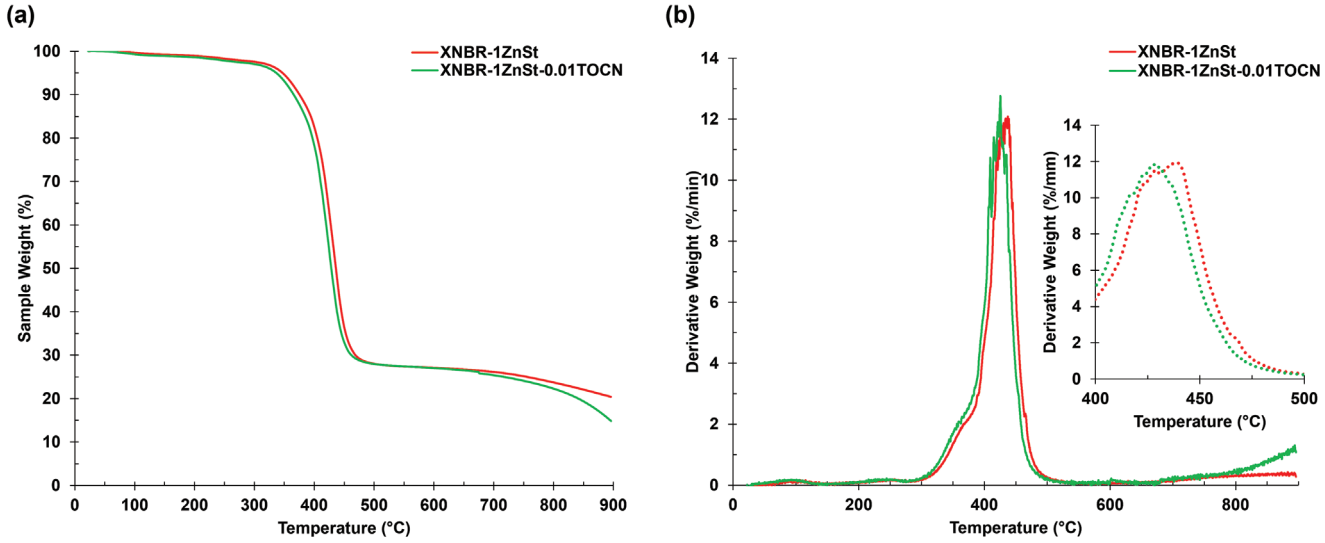

Figure 5. a) TGA curves and b) DTG curves of unfilled XNBR-1ZnSt and XNBR-1ZnSt-0.01TOCN, with magnified DTG curves ranging from 400 to 500 °C (inset).

Table 3. TGA results of XNBR composites.

Sample[a)]	Degradation Temperature [°C]	Temperature at 10% Weight Loss [°C]	Temperature at 50% Weight Loss [°C]	Carbon Residue [%]
XNBR-1ZnSt	437.26	375.42	436.26	20.41
XNBR-1ZnSt-0.01TOCN	425.45	365.73	428.54	14.82

[a)] XNBR-*m*ZnSt-*n*TOCN, where *m* and *n* represent the amount of ZnSt and TOCN (dry weight) added, respectively, measured in PHR.

With reference to **Figure 7a**, the XNBR chains may interact chemically with the compounding chemicals added to the formulation and carboxyl functional groups of TOCN. Chains of XNBR could interact with one another via covalent bonding at their C=C double bonds.[69] In addition, interactions exist via ionic bonding. This could be achieved by adding different zinc moieties, namely ZnO, ZDEC, and ZnSt, which possess the same metallic ions and can interact interchangeably with the XNBR rubber chain. Since XNBR contains carboxylate groups, they can also bind to zinc-ionized groups to form ionic pairs.[29,68] Combined with thermal stimulation, the dynamic and reversible nature of ions of opposing charges enhanced the self-healing properties of the formulated XNBR.[9] As demonstrated in this study, the addition of ZnSt has significantly impacted the strength recovery value of the material since it contributes to ionic interactions that are compatible with carboxyl groups along the chain. The compatibility of TOCN in providing additional sites for ionic and H-bonding was effective in promoting self-healing effects. However, although H-bonding is also reversible, ionic bonds remain dominant.

2.8. Proposed Self-Healing Mechanism

A proposed intrinsic self-healing mechanism for the XNBR composite matrix is illustrated in Figure 7a,b. When the XNBR material fractures, the zinc-based ionic networks are disrupted, leading to the creation of separate interfaces within the XNBR material. Despite these disruptions, the separated interfaces can be brought back into contact, initiating the self-healing process. This initiation is facilitated by opposing charge attractions, such as those between Zn^{2+} and OH^- ions contributed by either the XNBR chain, compounding chemicals, or TOCN filler, allowing for polymeric chain rearrangement and intermolecular diffusion at the damaged site. Over time, reconstructed ionic bonds, and subsequently a reversible network, could form, which can be further accelerated with the application of thermal energy.[30,48] The formation of carboxylic salts (i.e., zinc-based salts) behave as ionic cross-links, and at higher order aggregates, associates themselves as multiplets and clusters following the well-established Eisenberg model, which may be applied with other metal-based moieties that are compatible with the base polymer matrix.[30,68] Multiplets generally consist between six and eight dipole ions grouped to form larger structures, whilst retaining its dynamic reversible property.[8] Meanwhile, clusters are formed from associated multiplets and trapped chains, caused by electrostatic interactions. Restricted mobility of rubber chains with ionic groups could give rise to the formation of a separate hard phase, termed as ionic domains, bearing its own transition temperature.[70] Release of rubber chains during long-range ion hopping improves motion of rubber molecules in the system.[71] These ionic cross-links are mobile and dynamic, which promotes the self-healing property, unlike conventional covalent cross-linking. However, the formation of higher order structures or aggregates (such as clusters) have not been identified by dynamic mechanical analyzes (DMA) (Figure S3, Supporting Information). In this context, the self-healing mechanism is limited to ion hopping of

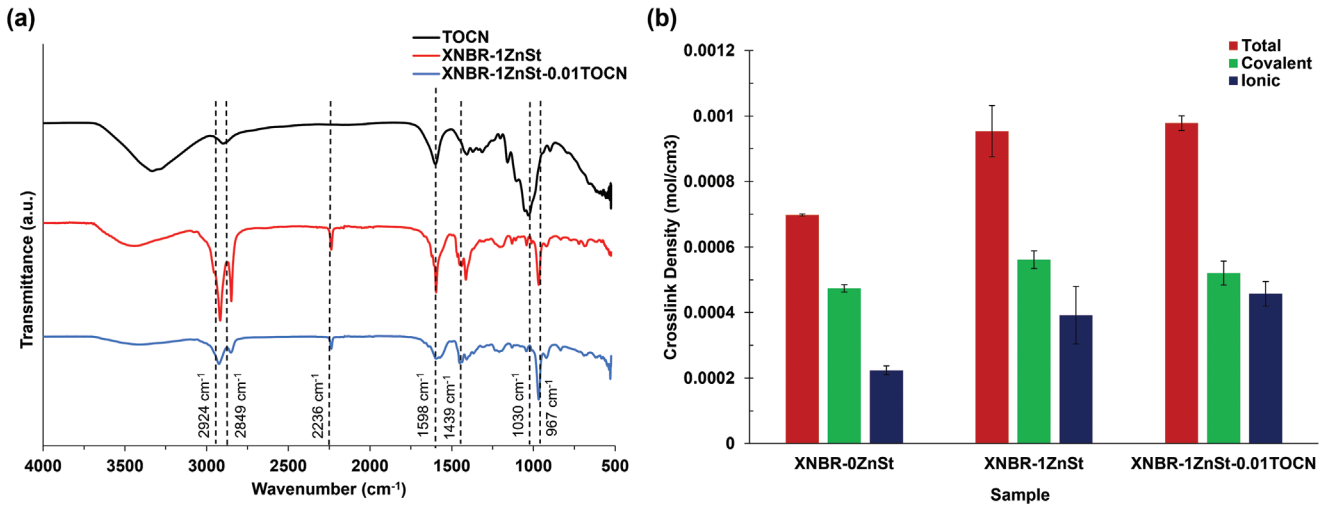

Figure 6. a) FTIR spectra of TOCN, XNBR-1ZnSt and XNBR-1ZnSt-0.01TOCN; b) Cross-link density results of XNBR-0ZnSt, XNBR-1ZnSt and XNBR-1ZnSt-0.01TOCN, sample size: n = 3.

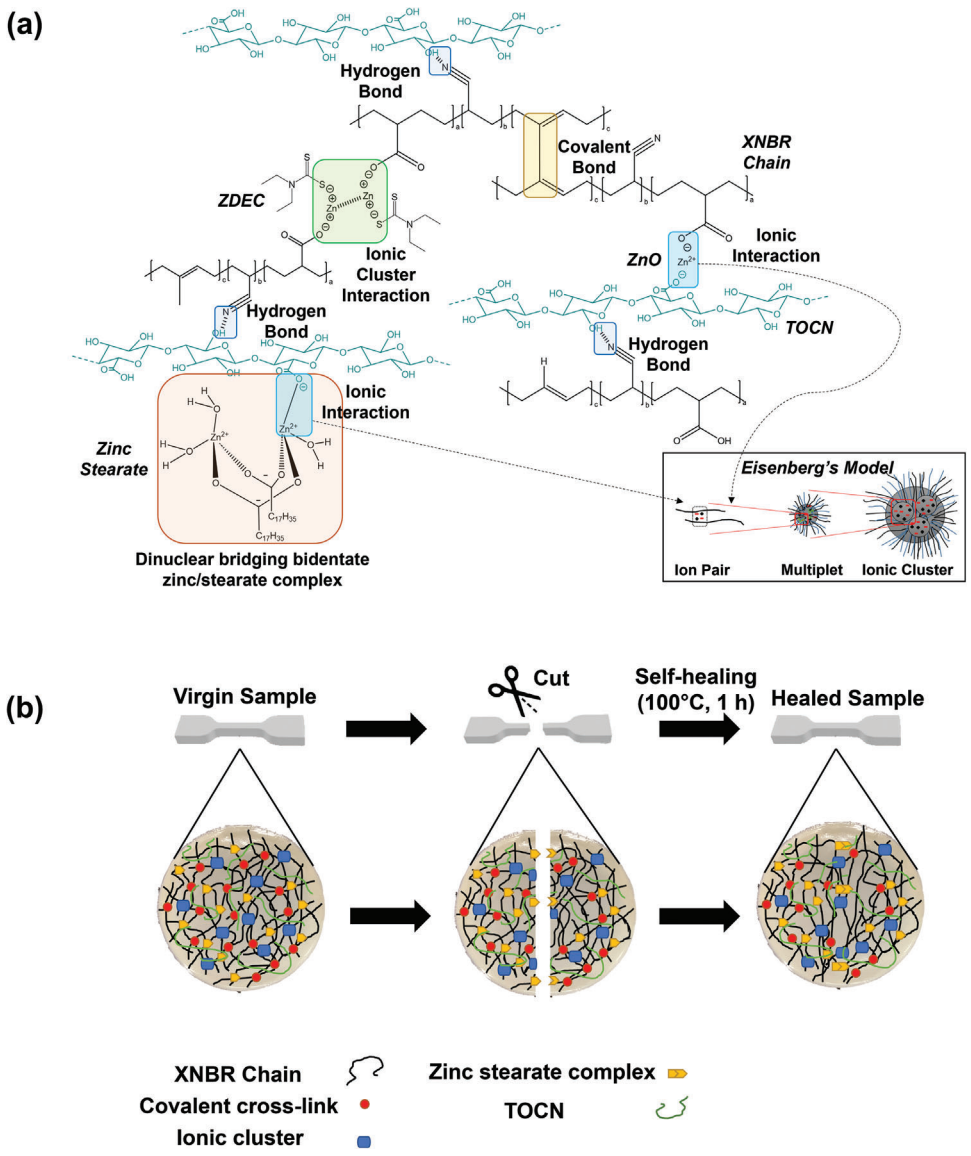

Figure 7. a) Interactions between compounding chemicals (i.e., ZnO, ZDEC and ZnSt), TOCN and XNBR polymer chains, and between XNBR chains themselves via covalent bonding; Eisenberg's model for ionomeric cluster formation (inset); b) Proposed self-healing mechanism of XNBR composite.

lower-order ionic interactions, namely ionic pairs. But, more research is needed to fully elucidate this finding.

In addition to the above-discussed mechanisms, weak reversible H-bonds (H—N) between TOCN and XNBR chains may also form. Besides acting as an effective lubricant to facilitate rubber chain interdiffusion, the significant role of ZnSt arises from its phase-changeable behavior, which immobilizes the XNBR chains during the healing process.[27] However, repeated healing at the same site may be limited by material exhaustion and ageing.[16] Despite this limitation, TOCN fillers do not independently contribute to bond reconstruction. Nevertheless, their interactions with the surrounding rubber chains and compounding agents enable them to play an effective role in continuously providing reinforcement effects at the unaffected regions of the material after self-healing, thus enhancing the magnitude of strength recovery. Overall, the proposed mechanism operates synergistically to repair the rubber matrix, resulting in high self-healing efficiency and prolonged material durability.

2.9. Fabrication of Lab-Scale Self-Healing Glove Prototype

To further evidence the feasibility of the self-healing XNBR composite, a laboratory-scale self-healing glove prototype was fabricated. Using the optimized latex formulation (XNBR-1ZnSt-0.01TOCN) and a retrofitted glove fabrication methodology, successful lab-scale prototypes were fabricated, as shown in **Figure 8a**. An incision was made with scissors on the palm area of the prototype and indicated (Figure 8b). Alongside a control prototype, they were then subjected to thermal self-healing (i.e., 100 °C for 1 h) before water and air leakage tests. As depicted in Figure 8c, no leakages were found in the healed glove, as

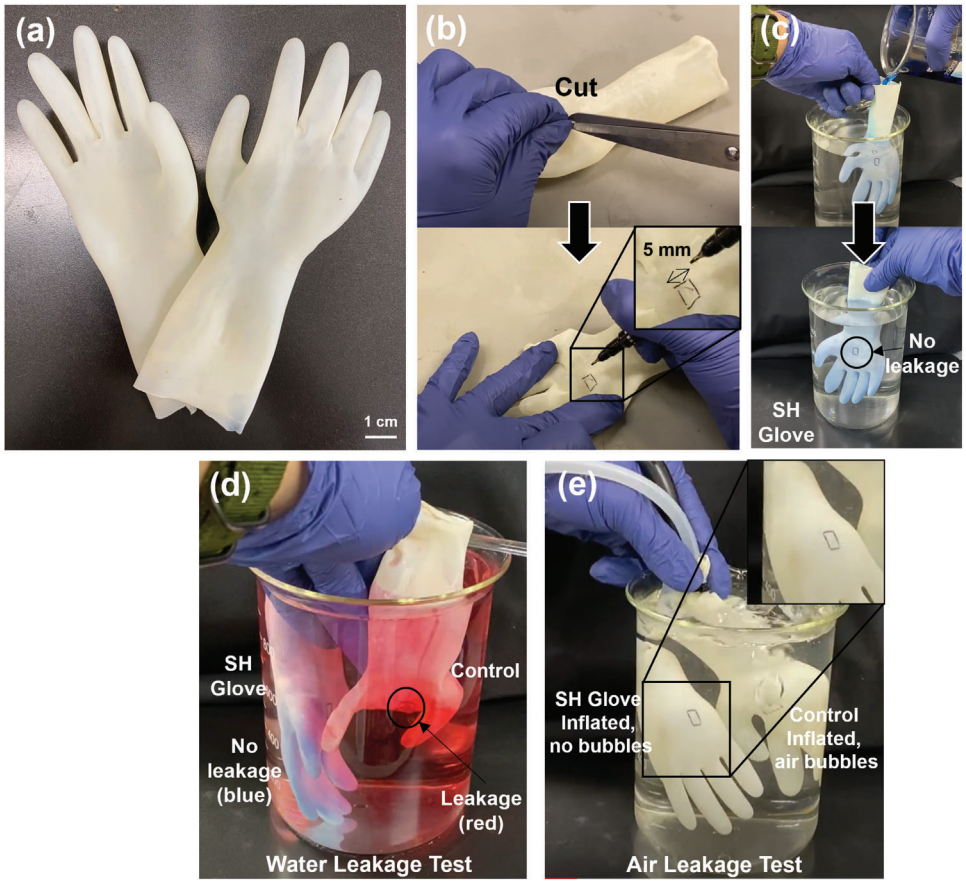

Figure 8. a) Fabricated self-healing (SH) glove prototype; b) Incision made on the palm area of glove prototype; c) No leakage of colored water (blue) in SH glove after healing; d) Leakage of colored water (red) in control glove; e) Inflated glove prototypes with no bubbles formed in the SH glove, and air escaping in control.

evidenced by the complete containment of the blue-colored water in the beaker upon filling. Meanwhile, for the negative control, it was clearly observed that there was insufficient self-healing achieved to seal the incision made, causing the red-colored water to leak out of the glove (Figure 8d). Additionally, from air leakage tests, it was further proven that the self-healed glove managed to be fully inflated without any leaks in the form of bubbles (Figure 8e). These observations suggest successful technology transfer from casting to dipping methods, showing feasibility for upscaling and industrial-scale production.

3. Conclusion

In this study, self-healing XNBR thin films and, subsequently, glove prototypes were successfully prepared and fabricated. Notably, this is the first study to report self-healing XNBR with a thickness under 1 mm with prototype feasibility validation. Self-healing behavior has been attributed to forming ionic interactions following the compounding of chemicals containing the zinc elemental moieties. It has been demonstrated that ZnSt concentration can further enhance self-healing efficiencies of the fabricated XNBR thin films by contributing to the formation of ionic networks as well as a "locking" material because of its reversible phase change properties. With 1 PHR of ZnSt concentration, self-healing efficiency was approximately 64%, corresponding to a recovered strength value of 4.53 MPa after thermal treatment at 100 °C for 1 h. About 50% of elongation recovery was achieved at the above-indicated healing conditions. Due to slight negative effects on initial tensile strength with ZnSt addition, the incorporation of a functionalized sustainable filler, namely TOCN, was shown to be effective in improving both the initial and recovered magnitudes of tensile strength, resulting in 72% self-healing efficiency with 5.38 MPa in magnitude. Furthermore, repeated self-healing cycles showed that the improved formulation exhibited 45% self-healing efficiency after three cycles. Microscopic images showing material recovery of the damaged site further evidenced the success of self-healing. Due to the presence of TOCN, the thermal stability of the composite was reduced, but its low concentration did not significantly affect it. This self-healing technology was successfully applied to fabricate a laboratory-scale glove prototype, which possesses self-healing properties and maintains a similar thickness of 0.40 mm. Subsequently, the prototype was subjected to water and air leakage tests. It was shown that the prototype managed to seal off the incision made, restricting leakage of water and air. It was envisaged that in addition to extending the service life of these gloves, this self-healing technology could also reduce waste and defects during manufacturing, thus minimizing waste and promoting

Table 4. Formulation recipe for self-healing XNBR composites.

Chemical	Concentration [PHR]	Role
XNBR, 45%	100	Base rubber
ZnO, 50%	5	Cure activator and cross-linker
ZDEC, 50%	1	Accelerator and cross-linker
ZnSt, 20%	0 to 5	Cure activator, anti-tacking agent
NaOH, 1M	As required	pH adjuster to pH 10
TOCN	0 to 0.50	Functionalized filler

materials sustainability on an industrial scale. Indeed, future research endeavors could investigate additional material properties such as tear strength and abrasion-deep resistance. Additionally, addressing challenges related to material ageing, adhering to commercial industry standard, and scaling up manufacturing processes would be crucial avenues to explore.

4. Experimental Section

Materials: XNBR latex (X6617) was provided by Synthomer Sdn. Bhd., Malaysia. The compounding chemicals of zinc oxide (ZnO) and zinc diethyldithiocarbamate (ZDEC) dispersions were sourced from Farben Technique Sdn. Bhd., Malaysia, while zinc stearate (ZnSt) dispersion was obtained from M&G Mixing Technologies Sdn. Bhd., Malaysia. Freeze-dried TEMPO-oxidized cellulose nanofibers (TOCN) (1.47 mmol COONa.g^{-1} dry CNF) were procured from the Process Development Center, University of Maine, USA. Toluene, chloroacetic acid, potassium hydroxide, calcium nitrate, and other chemical reagents were purchased from R&M Chemicals Sdn. Bhd., Malaysia.

Compounding Formulation of XNBR Self-Healing Composite: Wet-mixing was used to compound the XNBR composite, and the compounding recipe is given in **Table 4**. Each compounding agent was weighed separately and then poured into the XNBR latex while stirring at room temperature at 600 rpm. Afterward, the mixture was stirred continuously overnight to ensure homogeneity.

Preparation of Self-Healing XNBR Thin Films: Varying concentrations of up to 5 PHR of ZnSt dispersion were used to prepare the rubber composites. In the case of fabricated samples, they were designated as XNBR-*m*ZnSt, where *m* represents the amount of ZnSt incorporated during the compounding process (i.e., 0, 0.5, 1, 2, 3, 4, and 5 PHR). These samples were devoid of TOCN. After identifying the optimal ZnSt concentrations, nanocellulose fillers were introduced into the best formulation. These samples were labeled according to the convention XNBR-*m*ZnSt-*n*TOCN, where *n* represents the dry weight concentrations of TOCN (i.e., 0.01, 0.10, 0.20, and 0.50 PHR), added to the mixture after rehydration. Once the fillers were added, the mixture was homogenized at 3000 rpm for 2 min using a dispersing system (T25 Ultra-Turrax, IKA, USA). Following the completion of rubber latex compounding, approximately 16 mL of latex was pipetted into 115 mm-diameter glass Petri dishes. During preliminary tests, it was determined that thin films should possess a thickness of 0.40 ± 0.05 mm after curing. Two steps were involved in the curing process of the XNBR. The first step in the process involves a slow cure at 60 °C for 6 h to allow smooth gelation of the rubber latex. After this, an elevated temperature curing process (vulcanization) was conducted at 110 °C for 1 h.[37] After vulcanization, the thin films were easily removed from the Petri dishes and then cut into dumbbell shapes following ISO37-2 dimensions using a bench-scale hydraulic press and die cutter. A schematic flowchart of the method in preparing the XNBR thin films is attached in Figure S4 (Supporting Information).

Fabrication of Lab-Scale Self-Healing Glove Prototype: Fabrication of a lab-scale glove prototype follows the methodology of Supramaniam et al.[37] and Low et al.[72] with some modifications. Small ceramic hand formers procured from Gotaj Ceramics Sdn. Bhd., Malaysia, with a length of 15 cm, were used. The wet weight of latex used was 500 g, compounded with the optimized formulation determined from samples made via casting, as in Table 4. 20 wt.% of calcium nitrate was used as the coagulant. Due to the nature of the XNBR, no polymer coating was applied after vulcanization as the fabricated gloves could be easily stripped off the hand formers. Initially, all hand formers were thoroughly scrubbed with soap and water and left to dry in an aerated oven. Then, the formers were dipped into the coagulant mixture for 20 s. This was then followed by oven drying at 110 °C for 15 min, then left to cool to 60 °C. The formers were then dipped into the compounded latex for 20 s, followed by manual rotation to ensure even coating and thickness of the latex. Subsequently, the formers were dried in the oven at 110 °C until fully dried. The coagulation to latex dipping process was repeated for another cycle to achieve a glove thickness similar to that obtained during casting, which was comparable to a reusable glove. After the second latex dip, the formers were left to cure for 30 min at 110 °C. Finally, the formers were removed from the oven, left to cool, and subjected to a hot water leach at 70 °C to ease the stripping process, and then left to dry at ambient conditions. The same process was followed to produce a regular non-self-healing glove as a control for air and water leakage test validations.

Characterizations: Tensile strengths, strains, and moduli of the thin films were measured using a universal testing machine (INSTRON 5966, MA, USA) with a stretching speed of 500 mm.min^{-1} following ISO37 and ASTM-D412.[73,74] All samples were tested until failure and were performed in triplicate. In addition, the samples' initial tensile strength was quantified to determine their self-healing efficiency. Samples subjected to the cyclic healing protocol were designated as -SH*p*, where *p* represents the number of healing cycles executed within the scope of this study, with a maximum of three cycles.

Initially, the dumbbell-shaped samples were cut in the centre to determine the self-healing capacity of the films. The two fractured pieces were then brought into contact with one another and allowed to heal at 100 °C for 1 h in an aerated oven. Then, the samples were subjected to stress–strain tests and were performed in triplicate at the aforementioned stretching speed. To further demonstrate that the endowed self-healing property was not limited to a single instance of fracture at the same site, repeated cycles of up to three times of self-healing were also performed for each set of samples. As shown in Equation (1), self-healing efficiency can be expressed as the percentage of recovered tensile strength to the initial tensile strength.[37]

$$\text{Self} - \text{Healing Efficiency } (\%) = \frac{\text{Recovered Tensile Strength (MPa)}}{\text{Initial Tensile Strength (MPa)}} \times 100\% \quad (1)$$

The interactions between ZnSt and the nanocellulosic filler in the XNBR formulation were assessed using a Fourier-Transform infrared spectrometer (FTIR, Varian 600-IR series, Australia). The analysis involved 32 scans with a resolution of 4 cm^{-1}, spanning from 525 to 4000 cm^{-1}. With the aid of an optical microscope (Nikon Eclipse TS100, Nikon Instruments, USA), the surface of the fractured samples at the point of cut was viewed before and after self-healing. The field emission scanning electron

microscope (FE-SEM, Hitachi SU8010, Japan) operating at 5 kV was utilized to examine both the virgin surface morphology and the successful embedment of fillers within the samples. To increase conductivity and improve image clarity, samples were sputter-coated with an atomic layer of gold before morphological analysis.

As reported by Zainol et al.[25] and Supramaniam et al.[37] the cross-link density of the samples was determined using equilibrium swelling experiments. In each set, three samples were weighed and immersed in toluene at room temperature for 48 h. The samples were removed from toluene, gently blotted with filter paper to remove excess, and then weighed (m_1). In the next step, the samples were dried in an aerated oven at 60 °C until a consistent weight (m_2) was obtained. Flory–Rehner's equations (Equations (2) and (3)) were used to calculate the volume fraction of XNBR and cross-link density of the samples. The values represent the total number of cross-links (i.e., ionic and covalent). As part of the second and third stages of swelling, the samples were immersed in a mixture of toluene (95 vol.%) and 1 M chloroacetic acid (5 vol.%) for 48 h, followed by a further 48 h immersion in toluene. As a result, the ionic cross-links degraded independently.[75] The ionic cross-link density was the difference between the total and covalent cross-links, as shown in Equation (4).

$$\phi_r = \frac{\frac{m_2}{\rho_2}}{\frac{m_2}{\rho_2} + (m_1 - m_2)\,\rho_1} \tag{2}$$

$$-\left[\ln(1-\phi_r) + \phi_r + \chi\phi_r^2\right] = V_0\, n\left[\phi_r^{\frac{1}{3}} - \frac{\phi_r}{2}\right] \tag{3}$$

$$n_{ionic} = n_{total} - n_{covalent} \tag{4}$$

where ϕ_r = volume fraction of rubber in the swollen state, m_1 = weight of the sample in the swollen state, m_2 = weight of the sample in the dried state, ρ_1 = density of toluene, ρ_2 = density of XNBR, V_0 = molar volume of toluene, n = cross-link density, in terms of total, ionic, or covalent, represented by subscripts.

A thermogravimetric analyzer (TGA, Q50, TA Instruments, USA) was used to examine the thermal stability behavior of the fabricated XNBR composites at a rate of 10 °C.min^{-1} from 25 to 900 °C with nitrogen gas flow of 40 ml min^{-1} and purified air flow of 60 ml.min^{-1}.

Water and Air Leakage Tests: The self-healing properties of the fabricated self-healing glove prototype were validated via water and air leakage tests alongside a negative control made from natural rubber, as previously explored by Low et al.[72] First, an incision was made and marked on the palm area of the gloves. For water leakage tests, both the self-healing glove and control were filled with different colored water and then immersed into a beaker of water. For air leakage tests, a tube connected to a pressurized air outlet was inserted into the glove and then immersed into a beaker of water while being inflated. These tests were conducted at the start (point of cut) and after self-healing upon thermal stimulus exposure.

Statistical Analysis: Self-healing efficiencies were determined based on the ratio of means of recovered to initial tensile strengths. All other data were expressed as mean values ± standard deviation, with n = 3 per sample set, indicating triplicates during sample testing.

Supporting Information

Supporting Information is available from the Wiley Online Library or from the author.

Acknowledgements

The authors would like to specially thank Synthomer Sdn. Bhd., Malaysia, Farben Technique Sdn. Bhd., Malaysia and M&G Mixing Technologies Sdn. Bhd., Malaysia, for providing the dispersions for this study. D.Y.S.L. thanks Monash University Malaysia for the scholarship to support his PhD studies.

Open access publishing facilitated by Monash University, as part of the Wiley - Monash University agreement via the Council of Australian University Librarians.

Conflict of Interest

The authors declare no conflict of interest.

Data Availability Statement

The data that support the findings of this study are available from the corresponding author upon reasonable request.

Keywords

cellulose nanofibers, ionic interaction, self-healing glove, synthetic rubber, zinc stearate

Received: January 23, 2024
Revised: April 24, 2024
Published online: May 11, 2024

[1] H. Chittella, L. W. Yoon, S. Ramarad, Z.-W. Lai, *Polym. Degrad. Stab.* **2021**, *194*, 109761.
[2] Z. H. Boon, Y. Y. Teo, D. T.-C. Ang, *RSC Adv.* **2022**, *12*, 34028.
[3] D. Y. S. Low, S. Y. Tang, in *Elastomeric Nanocellulose Composites*, (Eds: S. Thomas, P. K. Mohamed, J. Kim, M. Tom), Woodhead Publishing, MA, USA, **2024**, p. 231.
[4] S. Pyay, W. Thanungkano, J. Mungkalasiri, C. Musikavong, *J. Clean. Prod.* **2019**, *237*, 117632.
[5] D. Y. S. Low, J. Supramaniam, A. Soottitantawat, T. Charinpanitkul, W. Tanthapanichakoon, K. W. Tan, S. Y. Tang, *Polymers* **2021**, *13*, 550.
[6] S. Sharib, A. Halog, *J. Clean. Prod.* **2017**, *141*, 1095.
[7] G. K. X. Poh, I. M. L. Chew, J. Tan, *Chem. Eng. Technol.* **2019**, *42*, 1771.
[8] S. Utrera-Barrios, R. Verdugo Manzanares, A. M. Grande, R. Verdejo, M. Á. López-Manchado, M. Hernández Santana, *Mater. Des.* **2023**, *233*, 112273.
[9] N. F. Mohd Sani, H. J. Yee, N. Othman, A. A. Talib, R. K. Shuib, *Polym. Test.* **2022**, *111*, 107598.
[10] J. Supramaniam, D. Y. S. Low, S. K. Wong, B. H. Goh, B. F. Leo, S. Y. Tang, *Sci. Rep.* **2022**, *12*, 4275.
[11] D. Y. S. Low, J. Supramaniam, W. D. Leong, A. Soottitantawat, T. Charinpanitkul, W. Tanthapanichakoon, S. Manickam, K. W. Tan, B. H. Goh, S. Y. Tang, *Mater. Today Sustain.* **2023**, *24*, 100545.
[12] S. Utrera-Barrios, R. Verdejo, M. Á. López-Manchado, M. Hernández Santana, *Eur. Polym. J.* **2023**, *190*, 112023.
[13] K. Yu, A. Xin, H. Du, Y. Li, Q. Wang, *NPG Asia Mater.* **2019**, *11*, 7.
[14] S. Utrera-Barrios, N. Steenackers, S. Terryn, P. Ferrentino, R. Verdejo, G. Van Assche, M. A. López-Manchado, J. Brancart, M. Hernández Santana, *Mater. Horiz.* **2024**, *11*, 708.
[15] A. M. Wemyss, C. Bowen, C. Plesse, C. Vancaeyzeele, G. T. M. Nguyen, F. Vidal, C. Wan, *Mater. Sci. Eng. R Rep.* **2020**, *141*, 100561.
[16] S. Islam, G. Bhat, *Mater. Adv.* **2021**, *2*, 1896.
[17] Z. Zhang, N. Ghezawi, B. Li, S. Ge, S. Zhao, T. Saito, D. Hun, P.-F. Cao, *Adv. Funct. Mater.* **2021**, *31*, 2006298.
[18] A. Cseke, M. Haines-Gadd, P. Mativenga, F. Charnley, *Proc. CIRP* **2020**, *90*, 473.
[19] S. Utrera-Barrios, R. Verdejo, M. A. López-Manchado, M. Hernández Santana, *Mater. Horiz.* **2020**, *7*, 2882.

[20] B. Li, P.-F. Cao, T. Saito, A. P. Sokolov, *Chem. Rev.* **2023**, *123*, 701.
[21] M. Das, A. R. Parathodika, P. Maji, K. Naskar, *Eur. Polym. J.* **2023**, *186*, 111844.
[22] S. W. Wajge, D. Basu, A. Das, S. Mandal, P. K. Maji, S. Singh, C. Das, *J. Polym. Sci.* **2024**, 1.
[23] M. Das, T. K. Sreethu, S. Pal, K. Naskar, *ACS Appl. Polym. Mater.* **2022**, *4*, 6414.
[24] S. M. Paran, G. Naderi, H. Mosallanezhad, E. Movahedifar, K. Formela, M. R. Saeb, *Polymers* **2020**, *12*, 1192.
[25] M. H. Zainol, Z. M. Ariff, M. F. Omar, T. M. Ping, R. K. Shuib, *J. Appl. Polym. Sci.* **2022**, *139*, 51948.
[26] D. Basu, A. Agasty, A. Das, S. Chattopadhyay, P. Sahu, G. Heinrich, *J. Appl. Polym. Sci.* **2020**, *137*, 48271.
[27] J. Araujo-Morera, M. A. López-Manchado, R. Verdejo, M. Hernández Santana, *Polymer* **2022**, *238*, 124399.
[28] A. Gupta, A. S., D. Basu, S. S. Banerjee, *Polymer* **2022**, *259*, 125321.
[29] K. Roy, S. C. Debnath, A. Pongwisuthiruchte, P. Potiyaraj, *ACS Omega* **2021**, *6*, 9975.
[30] M. Das, S. Pal, K. Naskar, *eXPRESS Polym. Lett.* **2020**, *14*, 860.
[31] S. W. Wajge, C. Das, *ACS Appl. Polym. Mater.* **2024**, *6*, 3094.
[32] X. Huang, A. Zhang, Q. Tan, K. Gou, Y. Chen, Y. Nie, G. Weng, *Macromolecules* **2024**, *57*, 963.
[33] K. Sasikumar, P. Jayesh, N. R. Manoj, T. Mukundan, D. Khastgir, *Polym. Compos.* **2018**, *39*, E1269.
[34] Y. Peng, S. Gu, Q. Wu, Z. Xie, J. Wu, *Acc. Mater. Res.* **2023**, *4*, 323.
[35] J. Xu, L. Zhu, Y. Nie, Y. Li, S. Wei, X. Chen, W. Zhao, S. Yan, *Materials* **2022**, *15*, 5993.
[36] S. Zechel, R. Geitner, M. Abend, M. Siegmann, M. Enke, N. Kuhl, M. Klein, J. Vitz, S. Gräfe, B. Dietzek, M. Schmitt, J. Popp, U. S. Schubert, M. D. Hager, *NPG Asia Mater.* **2017**, *9*, e420.
[37] J. Supramaniam, D. Y. S. Low, S. K. Wong, B. F. Leo, B. H. Goh, S. Y. Tang, *Chem. Eng. J.* **2022**, *437*, 135440.
[38] W. B. Setianto, H. Yohanes, Astuti, M., G. Atmaji, *IOP Conf. Ser.: Earth Environ. Sci.* **2022**, *963*, 012028.
[39] S. Mukhopadhyay, P. Sahu, H. Bhajiwala, S. Mohanty, V. Gupta, A. K. Bhowmick, *J. Mater. Sci.* **2019**, *54*, 14986.
[40] C. Xu, J. Nie, W. Wu, L. Fu, B. Lin, *Carbohydr. Polym.* **2019**, *205*, 410.
[41] S. Stein, A. Mordvinkin, B. Voit, H. Komber, K. Saalwächter, F. Böhme, *Polym. Chem.* **2020**, *11*, 1188.
[42] L. Cao, J. Huang, J. Fan, Z. Gong, C. Xu, Y. Chen, *Polym. Rev.* **2022**, *62*, 549.
[43] R. Blanchard, E. O. Ogunsona, S. Hojabr, R. Berry, T. H. Mekonnen, *ACS Appl. Polym. Mater.* **2020**, *2*, 887.
[44] J. M. Jardin, Z. Zhang, G. Hu, K. C. Tam, T. H. Mekonnen, *Int. J. Biol. Macromol.* **2020**, *152*, 428.
[45] G. Y. Yew, T. C. Tham, C. L. Law, D.-T. Chu, C. Ogino, P. L. Show, *Mater. Today Commun.* **2019**, *19*, 39.
[46] W. Liu, C. Xu, Y. Chen, *Compos. Sci. Technol.* **2023**, *234*, 109937.
[47] P. Das, A. Katheria, S. Ghosh, B. Roy, J. Nayak, K. Nath, S. Paul, N. C. Das, *Synth. Met.* **2023**, *294*, 117304.
[48] C. Dai, X. Cao, K. Gou, Q. Yin, B. Du, G. Weng, *J. Polym. Res.* **2021**, *28*, 97.
[49] P. Shaw, Z. Wei, Y. F. Goh (Synthomer Sdn. Bhd.), *U.S. 0282015*, **2022**.
[50] M. Das, T. R. Aswathy, S. Pal, K. Naskar, *Eur. Polym. J.* **2021**, *158*, 110691.
[51] S. Utrera-Barrios, J. Araujo-Morera, L. Pulido de Los Reyes, R. Verdugo Manzanares, R. Verdejo, M. Á. López-Manchado, M. Hernández Santana, *Eur. Polym. J.* **2020**, *139*, 110032.
[52] Y. Liu, K. Zhang, J. Sun, J. Yuan, Z. Yang, C. Gao, Y. Wu, *Ind. Eng. Chem. Res.* **2019**, *58*, 21452.
[53] S. Zhang, L. Han, H. Bai, C. Li, X. Wang, Z. Yang, M. Zai, H. Ma, Y. Li, *ACS Sustainable Chem. Eng.* **2021**, *9*, 8053.
[54] Q. Yan, L. Zhao, Q. Cheng, T. Zhang, B. Jiang, Y. Song, Y. Huang, *Ind. Eng. Chem. Res.* **2019**, *58*, 21504.
[55] N. L. Najwa Thajudin, M. H. Zainol, R. K. Shuib, *Polym. Test.* **2021**, *93*, 106975.
[56] C. Lin, Q. Wang, Q. Deng, H. Huang, F. Huang, L. Huang, Y. Ni, L. Chen, S. Cao, X. Ma, *Cellulose* **2019**, *26*, 4061.
[57] M. Prochon, *J. Therm. Anal. Calorim.* **2021**, *143*, 2933.
[58] P. G. Gan, S. T. Sam, M. F. Abdullah, M. F. Omar, *J. Appl. Polym. Sci.* **2020**, *137*, 48544.
[59] M. J. Lovato, L. J. del Valle, J. Puiggalí, L. Franco, *J. Funct. Biomater.* **2023**, *14*, 349.
[60] E. Barnes, J. A. Jefcoat, E. M. Alberts, M. A. McKechnie, H. R. Peel, J. P. Buchanan, C. A. Weiss Jr., K. L. Klaus, L. C. Mimun, C. M. Warner, *Polymers* **2019**, *11*, 1091.
[61] L. Qin, Y. Zhang, Y. Fan, L. Li, *Polym. Test.* **2023**, *120*, 107964.
[62] S. Krzemińska, L. Lipińska, M. Woluntarski, M. Oleksy, C. Ślusarczyk, W. Biniaś, A. Smejda-Krzewicka, *Polym. Bull.* **2020**, *77*, 1749.
[63] S. W. Wajge, C. Das, *Polym. Adv. Technol.* **2023**, *34*, 998.
[64] Y.-C. Liao, D.-G. Xu, P.-C. Zhang, *Nucl. Sci. Tech.* **2018**, *29*, 99.
[65] A. Laskowska, M. Zaborski, G. Boiteux, O. Gain, A. Marzec, W. Maniukiewicz, *eXPRESS Polym. Lett.* **2014**, *8*, 374.
[66] P. Zhang, F. Zhao, Y. Yuan, X. Shi, S. Zhao, *Polymer* **2010**, *51*, 257.
[67] D. D. Fleischmann, S. Ayalur-Karunakaran, F. Arbeiter, R. Schaller, A. Holzner, W. Kern, S. Schlögl, *Polym. Test.* **2018**, *66*, 24.
[68] A. Eisenberg, B. Hird, R. B. Moore, *Macromolecules* **1990**, *23*, 4098.
[69] D. Lenko, S. Schlögl, A. Temel, R. Schaller, A. Holzner, W. Kern, *J. Appl. Polym. Sci.* **2013**, *129*, 2735.
[70] S. Utrera-Barrios, R. Verdugo Manzanares, J. Araujo-Morera, S. González, R. Verdejo, M. Á. López-Manchado, M. Hernández Santana, *Polymers* **2021**, *13*, 3234.
[71] D. Basu, A. Das, K. W. Stöckelhuber, D. Jehnichen, P. Formanek, E. Sarlin, J. Vuorinen, G. Heinrich, *Macromolecules* **2014**, *47*, 3436.
[72] D. Y. S. Low, J. Supramaniam, A. H. Abd Rahim, S. Y. Tang, B. F. Leo, *J. Rubber Res.* **2021**, *24*, 631.
[73] ASTM D412-16, *Standard Test Methods for Vulcanized Rubber and Thermoplastic Elastomers - Tension*, ASTM international, West Conshohocken, PA **2021**.
[74] R. Ismail, N. H. B. Rajhan, H. A. Hamid, A. Ibrahim, *Data Br.* **2019**, *25*, 104166.
[75] Y. Liu, Z. Li, R. Liu, Z. Liang, J. Yang, R. Zhang, Z. Zhou, Y. Nie, *Ind. Eng. Chem. Res.* **2019**, *58*, 14848.